EXTRACTION OF GEOMETRICAL INFORMATION USED IN PHOTOVOLTAIC AND RAINWATER HARVESTING POTENTIAL ESTIMATION FROM UAV OPTICAL IMAGES

Caisse Amisse[1][2]
Alvaro Muriel Lima Machado[1]
Jorge Antonio Silva Centeno[1]

[1]Universidade Federal do Paraná
[2]Universidade Rovuma - Moçambique

ABSTRACT

Photovoltaic and rainwater harvesting assessment on rooftop has been studied extensively. Detailed methodologies are available over large study areas and designed to use data that are usually difficult and expensive to acquire. However, much less attention has been paid to the use of low-cost data for the estimation of photovoltaic parameters and rainwater collection in individual buildings. In this study, a workflow for extraction of geometrical information used in Photovoltaic and rainwater harvesting potential estimation from UAV optical images used to estimate photovoltaic and rainwater harvesting potential is presented. The optical images captured by the DJI Phantom 4 Unmanned Aerial Vehicle (UAV) were used to compute a point cloud, using state of the art Structure from Motion (SfM) algorithms. The modeling of the roof planes was made based on the spatial relationships between points using a Delaunay triangulation. From the generated model, roof geometrical parameters such as area, slope, and orientation were extracted and compared with reference measurements of Light Detection And Ranging (LiDAR) of the same scene. Statistical results from the experiments show that the SfM and LiDAR extracted parameters are very similar. The geometric parameters derived from UAV optical images can be used to support the analysis of the photovoltaic and rainwater harvesting potential in individual buildings. This method has the advantage to achieve results through the combination of low-cost technologies for data acquisition and processing, resulting in an easily reproducible methodology.

Keywords: Geometrical information, Photovoltaic, Rainwater.

RESUMO

Neste artigo é apresentada uma metodologia para extração de informação geométrica usada para estimativa do potencial fotovoltaico e coleta da água de chuva. A abordagem proposta usa câmeras a bordo de plataformas UAV para aerofilmagens e o processamento visando a geração de nuvem de pontos é feito usando algoritmos SfM. A modelagem dos planos do telhado é feita com base na relação espacial entre pontos vizinhos usando a triangulação de Delaunay. Do modelo gerado é extraída a informação geométrica do telhado (área, inclinação e orientação) e essa é comparada com as medidas de referência de uma nuvem de pontos LiDAR da mesma cena. Resultados estatísticos dos experimentos mostraram uma similaridade entre os parâmetros extraídos nas nuvens SfM e LiDAR. Os parâmetros geométricos derivados de imagens ópticas podem ser usados para tomada de decisão na análise de potencial fotovoltaico e coleta de água pluvial em telhados de edificações singulares. A principal vantagem do método é que o resultado é alcançado por meio da combinação de tecnologias de baixo custo para aquisição e processamento de dados, tornando a metodologia facilmente reprodutível.

Keywords: Informação geométrica, Fotovoltaico, Água pluvial.

1. INTRODUCTION

The growing energy demand has reinforced the research and use of alternative energy sources to reduce climate changes and avoid environmental problems. Solar energy is a valid alternative, which can be collected and converted into electric energy or heath for residential energy supply. This can be done by installing solar panels on the roof of buildings. Nevertheless, not all roofs are economically viable for solar energy, because of its size, orientation or slope. Information about the geometry of the roof is necessary to verify if it is suitable for solar energy collection. The size of a roof is also useful to compute the volume of rainwater intercepted by the roof, another alternative and environmental correct solution for water supply. Therefore, 3D information on the roof is needed for the evaluation of the potential photovoltaic production and/or rainwater harvesting. Economical and logistical constraints restrict the measurement of the extension and shape of the roof. Available methods include the use of aerial imagery, airborne LiDAR, and conventional topography. Nevertheless, buying an aerial survey or airborne LiDAR data of a building is too expensive. A topographic survey would be a viable option, but it may also be restricted by the available space around a high building. It also does not allow obtaining data of the rooftop. Recently, a new option became available and interesting, because of its lower cost and capacity to collect data of the rooftop. The use of UAV

enables collecting data that can be used to compute a point cloud of the roof applying photogrammetry and image processing. Analyzing the point cloud, it becomes possible to model the geometry of the roof.

To date, a number of representative surveys concerning roof modeling methods have been published in the literature, as summarized in various surveying articles (Brenner, 2005; Wang et al., 2018). Roof modeling methods can be divided on two main groups: a model--based and data-driven. Most of them are applied to LiDAR data but can be adapted to point clouds derived from images. The model-based methods aim at fitting a pre-defined template to the data, based on a collection of possible shapes stored in a library (Maas and Vosselman, 1999; Tarsha-Kurdi et al., 2007). In the data-driven method, segmentation algorithms are used to extract roof parts or edges in a previous step to shape modelling. There is no need for a specific library (Tarsha--Kurdi et al., 2007; Oude Elberink, 2008). One advantage of data-driven approaches is the capacity to adapt to different roof shapes. Examples can be found in the literature. For example, Joachim et al., (2009) detect roof planes in LiDAR data and then compute aspect, slope, and area of each roof facet. Then, it is carried out the photovoltaic potential analysis for each roof plane. Recent trends use a deep neural network method for roof segmentation (Pohle-Fröhlich, et al., 2019).

Some authors also rely on the combination of LiDAR data and other information sources. For example, Hujebri et al., (2013) or Awrangjeb et al., (2013) proposed the integration of LiDAR data and aerial imagery for roof modeling. Image segmentation algorithms were applied to extract the roof borders and break lines and then LiDAR data are used to extract the roof planes.

The use of aerial imagery instead of LiDAR data is a matter of research in recent literature. López-Fernández et al., (2015) describe an example, where RGB aerial images enable generating a 3D point cloud through photogrammetric and image processing algorithms. In a second step, segmentation is applied to the 3D point cloud for detection, extraction, and classification of roof planes. The roof planes are classified according to their theoretical productivity derived from their geometric characteristics (area, slope, and orientation). They also include thermographic information to locate obstacles for the installation of solar panels.

We propose an approach for the extraction of geometrical parameters used in photovoltaic and rainwater harvesting potential estimation that is cost-effective. To achieve this, we combine low-cost technologies for data acquisition with free software for data processing. The method is based on the use of unmanned aerial vehicles and the structure from motion approach and has great potential because of its lower cost when an individual building is analyzed within a project to

install solar panels and rainwater harvesting systems. An approach conceptually similar to ours has earlier been reported by lopes López-Fernández et al., (2015), but have not focused on low-cost sensors/ software and/or individual buildings. In the next section, the proposed method is introduced. Then, experiments with real data are presented to verify the proposed approach. Finally, conclusions and recommendations are outlined for further research.

2 METHODOLOGY

The methodology is summarized in four main steps presented in Figure 1: (1) Data collection (2) Pre-processing; (3) Point cloud processing, and (4) 3D modeling of roof elements and computation of geometric parameters used in the estimation of photovoltaic and rainwater harvesting potential.
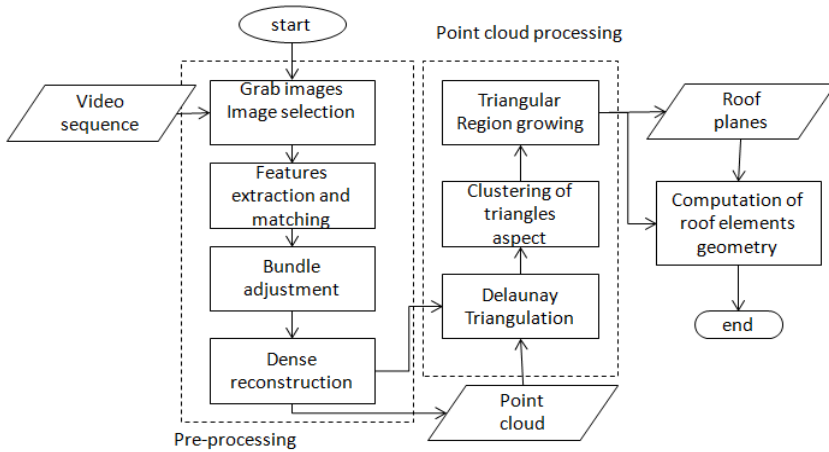
Figure 1 - Methodological flowchart

2.1 Data Collection and Pre-Processing

The aerial survey over the study area (Figure 2a) was carried out using the built-in camera of the small-sized four-axis DJI Phantom 4 quadrotor (Figure 2b). The DJI Phantom 4 is equipped with an onboard autopilot system, a compass, GPS and IMU sensors and a transmitter, a set that provides the position and altitude of the platform.
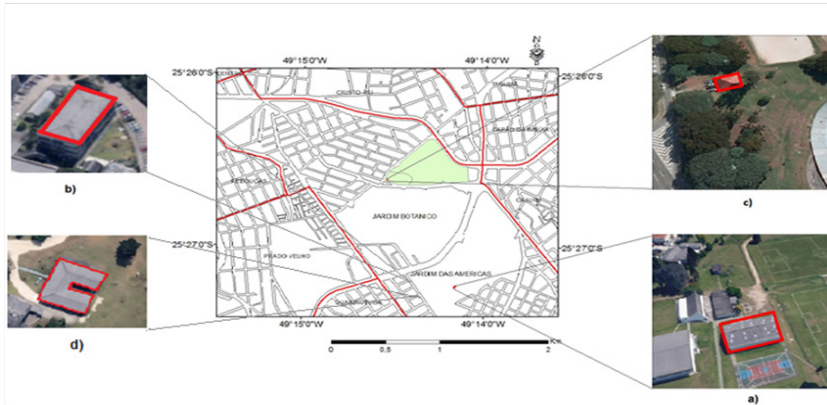
(a)

(b)

Figure 2 - (a) Location of the Study Area and (b) DJI Phantom 4 Quadcopter

The flight parameters were defined from the Equation 1:

$$GSD = \frac{H}{f} * \mu \qquad (1)$$

where GSD is Ground Sample Distance, H is the flight height (m), f the focal length (mm), and μ is the pixel size (mm). Flight planning was carried out using the Pix4D capture (available for IOS and Android systems), to define the route of the UAV for the data collection. The average flight height ranged between 20–40 meters (resulting in a mean GSD of 0.82 centimeters) and planned overlap of 80% lateral and 70% longitudinal. The images were visually inspected to discard poor images (i.e., blurred images).

2.2. Point cloud processing

It was computed a point cloud applying the structure from motion (SfM) approach, available in the VisualSFM (Wu, 2011) software, using the collected images. The pipeline includes:

(i) Features extraction and matching: In this step, homologous points are identified in neighboring images using the Scale Invariant Feature Transform (SIFT) algorithm (Lowe, 2004). The idea is to detect significant regions in the image and describe them with parameters that are invariant to scale rotation and illumination. The significant points, described by their parameters, are then compared to points detected in another image and similarity compatibility evaluated. If a point is detected in two images, the pair is matched. The Random SAmpling Consensus (RANSAC) algorithm (Fischler and Bolles, 1981) is applied to select the best matches and discard false pairs.

(ii) Bundle adjustment: The bundle adjustment is solved iteratively to reconstruct and refine the model starting with the pair of images with the largest number of good matches, and sequentially adding new images. The bundle adjustment adjusts a "bundle" of light rays that are leaving each 3D point towards each camera center and vice-versa (Ullman, 1979). It starts with an approximate solution for the camera pose and position and refines this solution by minimizing a cost function based on the difference between the projection of the feature points and the tracked features descriptors on the images (Triggs et al., 2000). The minimization is performed numerically using a non-linear least squares method, such as the Levenberg--Marquardt algorithm (Hartley and Zisserman, 2003). As a result, "correct" camera orientation (interior and exterior) and sparse 3D point cloud are obtained.

(iii) Dense reconstruction: In this step, it is increased the density of the point cloud based on the results of the bundle adjustment and the Patch-based Multi-view Stereo Software (PMVS), developed by Furukawa et al., (2010) and based on an algorithm for multiview stereopsis, that outputs a dense set of small patches covering the

visible surfaces in the images. This allows the PMVS algorithm (Furukawa and Ponce, 2010) to run dense reconstruction cluster-by--cluster and merge the results into a dense 3D point cloud. It must be taken into account that the point cloud generated by the Structure from Motion approach can fail on edge detection or present variations in density. This due to the repetitive effect of patterns and symmetries in the architecture of the scene (Wilson; Snavely, 2013; Cohen et al., 2012; Kosecka; Zhang 2010). Nevertheless, it allows computing a point cloud with a relatively low cost.

2.2.1 Quality assessment

The result was evaluated compared to a reference dataset, a cloud derived from an aerial LiDAR survey with an accuracy of 0.60 m. The computed point cloud was transformed into the same reference system as the reference point cloud (WGS-84), applying a 3D affine transform Equation 2. For this purpose, homologous points were selected in the reference and the computed point clouds. The parameters of the transform were estimated applying the Least Squares Method (LSM):

$$
\begin{bmatrix} X \\ Y \\ Z \end{bmatrix} = \begin{bmatrix} a_{11} & a_{12} & a_{13} & a_{14} \\ a_{21} & a_{22} & a_{23} & a_{24} \\ a_{31} & a_{32} & a_{33} & a_{34} \end{bmatrix} * \begin{bmatrix} X_0 \\ Y_0 \\ Z_0 \\ 1 \end{bmatrix}
\tag{2}
$$

where a11, a12, a13, ..., a34 are the parameters to be determined; X0, Y0, Z0 the coordinates in the original system and X, Y and Z the coordinates in the reference system. A direct point-to-point comparison is not possible, because the sets of points are different. Therefore, a triangulation was computed from the LiDAR point cloud and used as a reference surface. For each point in the SfM derived point cloud, the X, Y coordinates were used to find the triangle that encloses the point. Then, the height of this location in the triangulation was interpolated. The difference between the Z coordinate of the point and the interpolated Z coordinate of the triangulation was computed. Finally, the average and the root mean square error (RMSE) of the differences between the two models were obtained.

2.3 Roof modeling

The approach used to identify the roof planes is based on the analysis of local slope within the Delaunay triangulation computed from the point cloud. The triangulation is composed by vertices and edges, being the vertices the set of original points. The edges build up a triangle that links three neighboring points. Larger regions, composed of different contiguous triangles, are identified detecting neighboring triangles with similar gradient. The normal vector of each triangle is computed according to Equation 3:

$$ax + by + cz + d = 0 \tag{3}$$

a, b and c are the components of the normal vector to the plane, and d is the independent term.

We call aspect the relative orientation of the surface in relation to the north direction, which can be computed from the two first components of the normal vector, as shown in Equation 4 (López-Fernández, et al., 2015).

$$asp = \operatorname{atan}\left(\frac{b}{a}\right) \tag{4}$$

Although the aspect can assume any value between 0-360 degrees, it is expected that some angles are more frequent when a roof is composed by plane surfaces. Therefore, it is computed the relative frequency of the aspects to detect the most frequent angles. Each triangle is represented in a bi-dimensional space, representing the horizontal components of the normal vector (a, b). A clustering algorithm detects the most frequent directions according to a frequency threshold. In the end, each triangle is labelled according to the group in which it is included.

In the next step, adjacent triangles with the same label are grouped to build up a plane of the roof, applying the region growing algorithm. The process is summarized as follows: starting from a "seed" triangle, it is verified if at least one neighbor belongs to the same cluster of the seed. If yes, the region grows and the search repeated until the borders of the region are reached when no more neighboring triangles of the same cluster are found. A new seed triangle is chosen as the region stops growing. The region growing stops when all triangles are

grouped as roof faces.

2.3.1 Roof geometry

The set of neighboring triangles grouped in one region build up a plane, as described in the previous step, and are analyzed to compute geometric parameters that are necessary to study photovoltaic and rainwater catchment potential: slope, orientation, and area.

Orientation: Considering one group of triangles, as shown in figure 3, it is possible to compute the normal vector of each triangle, which has three components (a, b, c). The surface orientation is computed as the mean aspect of the set of triangles Equation 5.

$$ORIENT = \sum_{i=1}^{n} asp(i) \qquad (5)$$
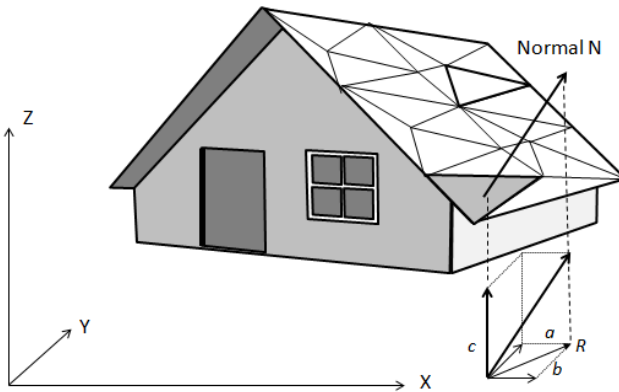
Figure 3 - Triangulation of a group of pixels representing a plane of the roof

Slope: The slope is the angle between the normal vector and the horizontal plane and is computed according to equations 6 and 7 (López-Fernández, et al., 2015). R stands for the size of the projection of the normal vector on the horizontal plane, as displayed in figure 3, and S for the slope

$$R = \sqrt{a^2 + b^2} \qquad (6)$$

$$S = \operatorname{atan}\left(\frac{c}{R}\right) \qquad (7)$$

In the final step, geometric analysis and classification were carried out considering the photovoltaic and rainwater harvesting potential. Roofs with areas smaller than the area needed for the installation of solar panels and areas facing the south are discarded because they are not well suited in the southern hemisphere. Ideal roofs for photovoltaic production are those with north orientation or that accept an angular variation of 45° to the east or west.

To estimate the rainwater harvesting potential, all the roofs were taken as potentials, as the roof orientation is not decisive for the rainwater harvesting assessment.

3. RESULTS AND DISCUSSION

This section presents the results obtained in our experiments. Figure 4 illustrates an example of the UAV trajectory and the camera pose during the flight as color triangles.

Figure 4 - Point clouds with camera poses

A dense point cloud is obtained (figure 5) applying the SfM method. Spurious points were filtered out to eliminate points that do not belong to the roof, such as points on antennas, chimneys, ground or trees.
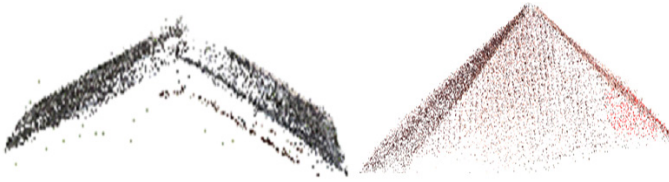
Figure 5 - Filtered point clouds for the experiments 1 (a) and 2 (b)

Based on the filtered point clouds, roof planes were modelled based on the triangulation and slope/aspect variations. Figure 6 shows the results of the region growing on four roof examples. The first one is very simple, with two planes. The second and third have four planes and the last six. When dealing with the second example, Figure 6b, it was noticed that the method fails at the top of the roof. This fact can be explained by the lack of points in such regions, as it can be seen in figure 5b and by the difficulty to determine the right aspect. In the third example, figure 6c, and 6d, some errors in the reconstruction at the edges of the roof planes are visible. As most errors are located at the borders, it was considered that they would not influence the result significantly. It was also noticed that the sources of the main errors are blurred images and errors in the generation of the point cloud by SfM.

(a)

(b)

(c)

(d)
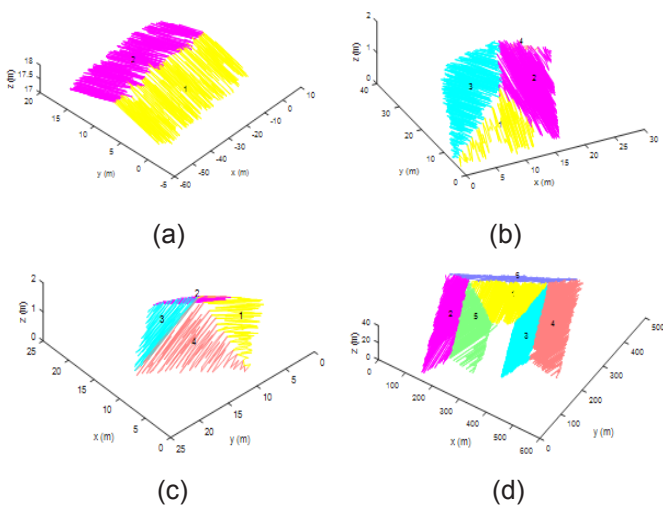
Figure 6 - Roof model showing the modelled roof planes for experiments 1(a), 2(b), 3(c) and 4(d)

For quality assessment the registration was conducted by using 3D affine coordinate transformation, equation (2). For experiment 1, six points were considered in the SfM and LiDAR point clouds; six, five and ten points for experiments 2, 3 and 4 respectively (an example is displayed in Figure 7). The solution of the transformation was obtained by adjustment using the LSM.
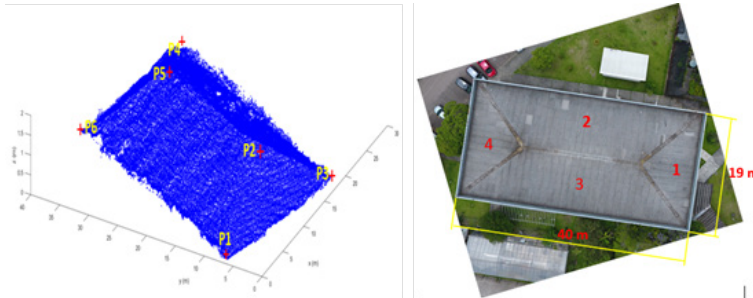
Figure 7 - Point cloud registration and reference dimensions

Figure 8 illustrates a comparison between the LiDAR and SfM derived point clouds. Although the results are very similar, errors can be noticed in the comparison. Nevertheless, the roofs are parallel and agree in dimensions. Errors are expected, because it is difficult to identify the corners in the point clouds. In some cases, especially in the first and second example, the SfM software produced a point cloud with height variations.

(a)   (b)   (c)   (d)
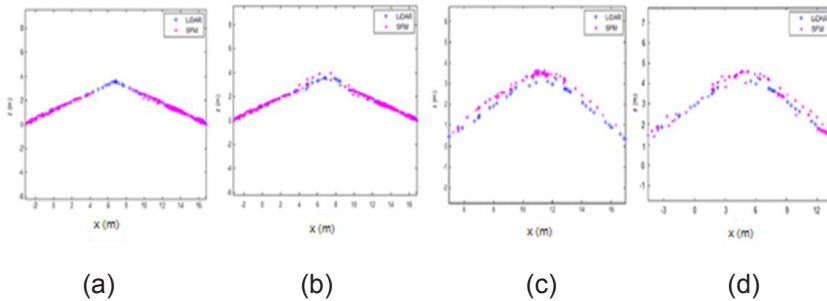
Figure 8 - Registry comparison between SfM and LiDAR point clouds

The discrepancies between the SfM point cloud and the reference point cloud were computed to assess the similarity between the point clouds (Figure 9). As the histograms illustrate, the most frequent differences are close to zero. The residual best fit was achieved in the first example (Figure 9a), with a mean of 0.02 m and a standard deviation of 0.15 m. In the second, third and fourth histograms (Figure 9b, c, d), the mean differences are 0.25 m, 0.01 m, and 0.04 m, and the standard deviation of 0.35 m, 0.58 m and 0.2 m respectively, which means that the fit was not as good as the first one. The larger differences can be explained by the texture variation in the point cloud derived using the UAV data.

(a)　　　　　　(b)　　　　　　(c)　　　　　　(d)
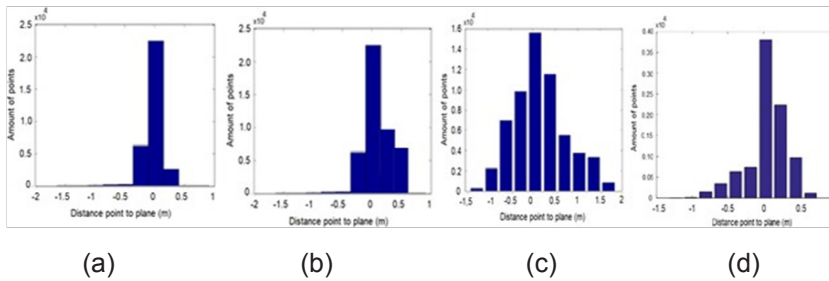
Figure 9 - Residues histogram

3.1. Area slope and orientation

The point clouds were segmented to separate the planes of the roofs and compute their Area, Slope and Orientation (aspect). The same parameters were obtained from the reference point cloud, by visual delineation of the roof planes. A comparison is shown in Table 1. Concerning the area, the comparison suggests that the errors can range, from 1.00 - 1.67%. The reason for the larger errors (1.67%) is the quality of the SfM point cloud, concerning to errors in edge detection (Kosecka; Zhang 2010; Cohen et al., 2012; Wilson; Snavely, 2013). As the point cloud of the fourth roof has less texture, the areas are correctly segmented. When there is texture (local height variation) in the point cloud, the region- growing algorithm fails to group the triangles of a plane.

Table 1 - Summary of extracted parameters (Area, Slope, Orientation) and Differences

		Parameters							**Differences**		
		Area (m2)		**Slope (o)**		**Orientation (o)**					
	Roofing	Ref.	SfM	LiDAR	SfM	LiDAR	SfM	Area (%)	Slop (%)	Or (%)
Exp 1	Face 1	291	289.97	58.66	57.89	54	53.70	0.35	1.31	0.56
	Face 2	291	289.95	58.66	57.87	54	53.70	0.36	1.35	0.56
Exp 2	Face 1	75	74.62	16.4	16.17	52	51.75	0.51	1.40	0.48
	Face 2	125	124.3	16.5	16.31	52	51.75	0.56	1.15	0.48
	Face 3	125	124.4	16.5	16.31	52	51.75	0.48	1.15	0.48
	Face 4	75	74.58	16.4	16.18	52	51.75	0.56	1.34	0.48
Exp 3	Face 1	21.51	21.38	56.72	55.95	48	47.63	0.60	1.36	0.77
	Face 2	20.88	20.76	56.72	55.95	48	47.63	0.57	1.36	0.77
	Face 3	21.51	21.38	56.72	55.95	48	47.63	0.60	1.36	0.77
	Face 4	20.88	20.76	56.72	55.95	48	47.63	0.57	1.36	0.77
Exp 4	Face 1	30.56	30.41	15.24	15.08	43	42.71	0.49	1.05	0.67
	Face 2	64.03	63.87	15.47	15.28	55	54.62	0.25	1.23	0.69
	Face 3	38.07	37.99	15.28	15.11	55	54.62	0.21	1.11	0.69
	Face 4	64.03	63.87	15.15	14.98	55	54.62	0.25	1.12	0.69
	Face 5	38.07	37.98	15.46	15.28	55	54.62	0.24	1.16	0.69
	Face 6	60.06	59.83	15.11	14.94	43	42.71	0.38	1.13	0.67

On the other hand, the slope differences are lower (1.05-1.40%), which means that the method is well suited to estimate the slope. This is explained by the fact that the region growing method, even when it does not find the whole region, it can group triangles of the same plane with success. The same happens in the case of the orientation (aspect). The differences lie around 0.48 - 0.77%. It is worth noting that the discrepancies are related to errors in the segmentation of the roof planes at the edges. This is related to the lack of points at roof edges and on the ridge.

4. CONCLUSIONS

This study has demonstrated a simple method to extract geometric parameters used in photovoltaic and rainwater harvesting potential estimation of individual buildings based on 3D point clouds computed from UAV optical images. The method, while relatively simple, does yield a comparatively accurate estimation of the geometric parameters. The method provides a semi-automatic, quick and accurate evaluation of isolated roofs without the need of consulting the technical documentation of the building, avoiding subjective evaluations performed by a human operator.

The experimental results confirm that the proposed method can extract geometric parameters such as area, slope, and orientation. For the analysis of the photovoltaic potential, the method is promising, because slope and orientation were computed with relatively good accuracy in a cost-effective manner. The method failed to compute the area with enough accuracy because the segmentation of the roof planes failed. Nevertheless, this problem can be solved by computing the intersection of the detected planes, because, as the slope and orientation results show, the planes are estimated with enough accuracy. This step was not performed here. The area also affects the estimation of the available rainwater.

Further research is required to evaluate how point cloud registration using planar or linear features can improve the results and the effect that such steps can improve the computation of geometrical parameters.

5. ACKNOWLEDGEMENT

REFERENCES

AWRANGJEB, M.; ZHANG, C; FRASER, C S. Automatic extraction of building roofs using LIDAR data and multispectral imagery. ISPRS journal of photogrammetry and remote sensing, v. 83, p. 1-18, 2013.

BRENNER, C. Building reconstruction from images and laser scanning. International Journal of Applied Earth Observation and Geoinformation, v. 6, n. 3-4, p. 187-198, 2005.

COHEN, A., ZACH, C., SINHA, S. N., POLLEFEYS, M. Discovering and exploiting 3d symmetries in structure from motion. In: 2012 IEEE Conference on Computer Vision and Pattern Recognition. IEEE, 2012. p. 1514-1521.

FISCHLER, M. A.; BOLLES, R. C. Random sample consensus: a paradigm for model fitting with applications to image analysis and automated cartography. Communications of the ACM, v. 24, n. 6, p. 381-395, 1981.

FURUKAWA, Y., CURLESS, B., SEITZ, S. M., SZELISKI, R. Towards internet-scale multi-view stereo. In: 2010 IEEE computer society conference on computer vision and pattern recognition. IEEE, 2010. p. 1434-1441.

FURUKAWA, Y; PONCE, J. Accurate, dense, and robust multiview stereopsis. IEEE transactions on pattern analysis and machine intelligence, v. 32, n. 8, p. 1362-1376, 2010.

HARTLEY, R; ZISSERMAN, A. Multiple view geometry in computer vision. Cambridge university press, 2003.

HUJEBRI, B; SAMADZADEGAN, F; AREFI, H. Fusion of ALS Point Cloud and Optical Imagery for 3D Reconstruction of Building's Roof. ISPRS Archives–Volume XL-1/W3, 2013, v. 40, p. 197-201, 2013.

JAMES, M. R.; ROBSON, S. Mitigating systematic error in topographic models derived from UAV and ground-based image networks. Earth Surface Processes and Landforms, v. 39, n. 10, p. 1413-1420, 2014.

JOCHEM, A., HÖFLE, B., RUTZINGER, M., PFEIFER, N. Automatic roof plane detection and analysis in airborne lidar point clouds for solar potential assessment. Sensors, v. 9, n. 7, p. 5241-5262, 2009.

KOŠECKÁ, J; ZHANG, W. Extraction, matching, and pose recovery based on dominant rectangular structures. Computer Vision and Image Understanding, v. 100, n. 3, p. 274-293, 2005.

LÓPEZ-FERNÁNDEZ, L., LAGÜELA, S., PICÓN, I., GONZÁLEZ-AGUILERA, D. Large scale automatic analysis and classification of roof surfaces for the installation of solar panels using a multi-sensor aerial platform. Remote Sensing, v. 7, n. 9, p. 11226-11248, 2015.

LOWE, D. G. Distinctive image features from scale-invariant keypoints. International journal of computer vision, v. 60, n. 2, p. 91-110, 2004.

MAAS, H. G., VOSSELMAN, G. Two algorithms for extracting building models from raw laser altimetry data. ISPRS Journal of photogrammetry and remote sensing, v. 54, n. 2-3, p. 153-163, 1999.

POHLE-FRÖHLICH, R.; BOHM, A.; UEBERHOLZ, P.; KORB, M.; GO-EBBELS, S. Roof Segmentation based on Deep Neural Networks. In: VISIGRAPP (4: VISAPP). 2019. p. 326-333.

ELBERINK, S. O. Problems in automated building reconstruction based on dense airborne laser scanning data. International Archives of Photogrammetry, Remote Sensing and Spatial Information Sience, v. 37, p. B3, 2008.

TARSHA-KURDI, F.; LANDES, T.; GRUSSENMEYER, P.; KOEHL, M. Model-driven and data-driven approaches using LIDAR data: Analysis and comparison. 2007.

TRIGGS, B.; MCLAUCHLAN, P. F.; HARTLEY, R. I.; FITZGIBBON, A. W. Bundle adjustment - a modern synthesis. In: International workshop on vision algorithms. Springer, Berlin, Heidelberg, 1999. p. 298-372.

ULLMAN, S. The interpretation of structure from motion. Proceedings of the Royal Society of London. Series B. Biological Sciences, v. 203, n. 1153, p. 405-426, 1979.

WANG, R; PEETHAMBARAN, J; CHEN, D. LiDAR point clouds to 3-D Urban Models: a review. IEEE Journal of Selected Topics in Applied Earth Observations and Remote Sensing, v. 11, n. 2, p. 606-627, 2018.

WILSON, K; SNAVELY, N. Network principles for sfm: Disambiguating repeated structures with local context. In: Proceedings of the IEEE International Conference on Computer Vision. 2013. p. 513-520.

WU, C. VisualSFM: A visual structure from motion system. 2011.